Received: 18 December 2020 | Revised: 30 March 2021 | Accepted: 2 April 2021

DOI: 10.1002/pc.26068

RESEARCH ARTICLE

Polymer COMPOSITES WILEY

Nonlocal heat conduction in single-walled carbon nanotubes

Amin Pourasghar[1,2] | **Wenzhi Yang**[1] | **Domiano Pasini**[2] | **Zengtao Chen**[1]

[1]Department of Mechanical Engineering, University of Alberta, Edmonton, Alberta, Canada

[2]Department of Mechanical Engineering, McGill University, Montreal, Quebec, Canada

Correspondence
Amin Pourasghar, Department of Mechanical Engineering, University of Alberta, Edmonton, AB T6G 2G8, Canada.
Email: pourasgh@ualberta.ca

Abstract

This paper explores how reinforcing the hyperbolic heat conduction by the nonlocality affects temperature distribution in nanostructures such as nanobeam and single-walled carbon nanotubes (SWCNTs). The work dissects the nonlocal heat conduction by advocating a thoroughly new application of the differential quadrature method. The nanobeam is modeled like a SWCNT (cylindrical shell), and the boundaries on the inner and outer sides are considered under a temperature jump at the nanoscale. The effects of several parameters on the temperature distribution through the thickness of the nanobeam are highlighted, including time-dependent boundary conditions, time lag, nonlocal parameter, length, and radius of the hollow beam.

KEYWORDS

differential quadrature method (DQM), hyperbolic heat conduction, nanobeam, nonlocal heat conduction, SWCNT

1 | INTRODUCTION

Over the last decade, nanostructures have attracted much interest due to their astounding characteristics that influence electrical, physical, chemical, optoelectrical, and biological properties. Carbon nanotubes (CNTs), one of the most popular carbon-based devices, have been investigated thoroughly over the past several decades for their potential applications including field-effect transistors, interconnects, electron field emitters, sensors, and energy storage and energy conversion devices.[1–4] Although the thermal conductivity of polymer matrix reinforced by CNTs improves when CNTs are randomly distributed, due to their large aspect ratio and the strong Van der Waals force between the CNTs and the medium, they tend to aggregate and form clusters in the nano-composite.[5,6]

Many studies about CNTs and nanoscale structures were based on the classical continuum theory, which ignores the size effect. To tackle this problem, nonlocal elasticity theories were introduced for nanoscale structures to develop size-dependent relations.[7–12] These approaches show superior performance in coping with this problem than any other approach. Furthermore, several works studied the heat conduction in nanocomposites,[13–17] and nanostructures theoretically[18–21] and experimentally.[22–24]

In the classical model, the temperature gradient of a specific point causes the heat flux at the same point. At the nanoscale, a sufficient number of collisions among energy carriers are required for the heat transport to take place.[25,26] In general, quantifying the value of a physical property at one point through another physical property in a region near to that point is considered as the nonlocal effect in the continuum theory and has been observed experimentally.[27]

The hyperbolic heat conduction equation is introduced based on the Cattaneo and Vernotte model for the heat flux incorporating a relaxation mechanism that gradually adjusts to a change in the temperature gradient.[28–32] This model is a satisfactory extension of the classical diffusion theory and can yield the hyperbolic wave equation within the continuum assumption. Based on the investigations of Soboley[32] and Tzou,[33] since

the heat flux at micro/nano scale is substantially nonlocal, classical models should be modified by introducing the characteristic length of the material. Prior research generally confirms that at the nanoscale, the heat transfer is quite different from that estimated by classical laws. To tackle this problem, Guyer and Krumhansl (GK)[34,35] introduced a generalized model by considering the characteristic length of the material as follows:

$$q(z,t+\tau_q) = -k\nabla T(z,t) + l^2\nabla^2 q(z,t), \tag{1}$$

where τ_q and l are the time lag of the heat flux and internal characteristic length, respectively. To investigate the transient heat conduction from nano- to macro-scales, Wang et al.[36] considered the effects of both the non-Fourier heat conduction and the nonlocality of the problem simultaneously. Xu[37] investigated the nanoscale heat conduction in silicon thin films by considering the temporally and spatially nonlocal effects. They showed thermal wave propagation in nanoscale materials.

Employing the differential quadrature method (DQM) to solve the transient or time-dependent problems is a challenging problem in solid mechanics. There have been a few reports of implementing DQM to discretize the spatial domain and one of them employing finite difference, using the Runge Kutta or Newton–Raphson method, to discretize the temporal domain.[38,39] Instability is the most crucial drawback of this method.[40] There have been a few studies that seek to discretize the temporal domain using DQM.[41,42] Block marching is an efficient method to solve a time-dependent problem.[43–45]

To solve the hyperbolic and dual-phase-lag heat conduction, Pourasghar and Chen[44,46,47] introduced a new application for the DQM. They discretized the spatial and temporal domain by DQM. Finally, they implemented the Newton–Raphson method to obtain the temperature history along with the temperature distribution through the thickness of the material. It has been recognized that the DQM has the capability of producing highly accurate solutions with minimal computational effort[43] when the method is applied to problems with globally smooth solutions. The main advantages of the DQM are its inherent conceptual simplicity and the fact that easily programmable algorithmic expressions are obtained.

A novel contribution of this study is to propose a new approach to accommodate both the temperature nonlocality and phase lagging, by modifying the non-Fourier heat conduction introduced in Ref [35], and solving the problem by DQM.[8,38] The proposed method marches in the time direction block by block. In each block, there are several time levels, and the numerical results at these time levels are obtained simultaneously. With this strategy, the numerical solution at the $(n+1)$th time level depends on the solutions of the previous levels from the 1st to the nth levels. The results in the temporal domain are obtained using the Newton–Raphson method. Finally, in this paper we do not witness any unrealistic value of overshooting for temperature as both temperature nonlocality and phase lagging are accommodated in the heat conduction equation.

2 | NONLOCAL HEAT CONDUCTION

Cattaneo[28] and Vernotte[29] proposed the classical thermal wave model, in which the increase of the heat flux vector is considered due to the phonon collision in a duration of the relaxation time (τ_q):

$$q + \tau_q \frac{\partial q}{\partial t} = -k\nabla T. \tag{2}$$

where q is heat flux vector, t is time, k is thermal conductivity, T is temperature, and ∇ is gradient operator. Even though the hyperbolic models have shown that the introduction of the phase-lag of the temperature gradient may avoid the discontinuity of the temperature distribution, these models are unstable and share overshooting temperature.[45] In order to provide a realistic distribution of temperature and resolve the issues, we used modified version of the Hyperbolic heat conduction in which one more mechanism for the heat transfer, acting at the scales L, comparable with the phonon free path l is included.[34,35] This, in turn, leads to a minimized overshooting temperature, thus being able to get much closer to the realistic conditions. The following equation shows the participation of the energy carriers into the heat conduction relation by l:

$$\left[1-(l)^2\nabla^2\right]q = -k\frac{\partial T}{\partial z} \tag{3}$$

where z is the thickness direction as shown in Figure 1 and l is the mean free paths of phonons, which makes the temperature at one specific point a function of the temperature of all points in the body. As mentioned earlier, the modified form of the non-Fourier heat conduction is used[35]:

$$\left[1-l^2\nabla^2+\tau_q\frac{\partial}{\partial t}\right]q = -k\frac{\partial T}{\partial z} \tag{4}$$

where τ_q reflects the effects of thermal inertia.

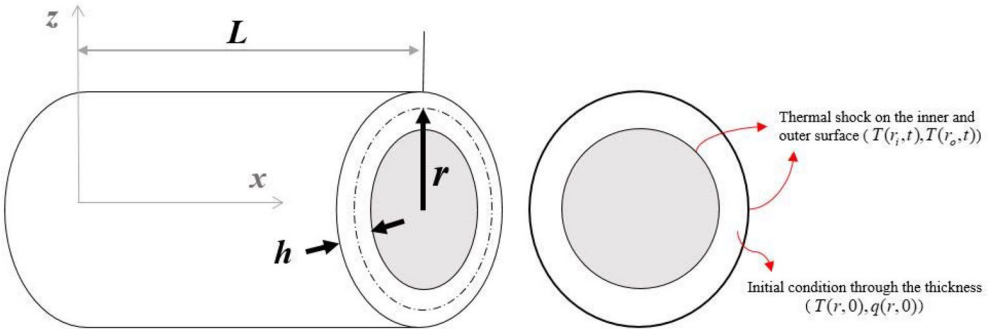

FIGURE 1 Single-wall carbon nanotube (SWCNT) modeled as a nonlocal Timoshenko nanobeam [Color figure can be viewed at wileyonlinelibrary.com]

2.1 | Nonlocal heat conduction analysis of CNTs

Fourier and non-Fourier heat conduction models, such as hyperbolic and dual-phase-lagging heat conduction, do not accommodate the size effect, while the GK model reflects both the nonlocal and phase lagging effects[34,35,49–51]:

$$q+\tau_q\frac{\partial q_z}{\partial t}=-k\frac{\partial T}{\partial z}+l^2\left(\frac{\partial^2 T}{\partial z^2}\right). \tag{5}$$

Furthermore, from the first law of thermodynamics, the conservation of energy takes the following form:

$$C_p\frac{\partial T}{\partial t}+\frac{\partial q}{\partial z}=g(z,t) \tag{6}$$

with C_p being the volumetric heat capacity, $C_p=\rho c$.

Let us consider a SWCNT, as shown in Figure 1, which is subjected to a heat shock at the inner or outer surfaces. A SWCNT is modeled as a Timoshenko nanobeam with radius r, length L, and effective tube thickness h.

The temperature fields in the above equations can be obtained from nonlocal heat conduction and energy equation as follows:

$$q+\tau_q\frac{\partial q_z}{\partial t}=-k\frac{\partial T}{\partial z}+l^2\frac{\partial^2 T}{\partial z^2} \tag{7}$$

$$\rho C\frac{\partial T}{\partial t}+\frac{\partial q}{\partial z}=g(z,t), \tag{8}$$

where $g(z, t)$ is the heat source, which is taken to be zero in this paper.

For thermal boundary conditions, it is assumed that the SWCNT is under a sudden temperature change on the outer surface ($z=-\frac{h}{2}$) and all other boundaries are considered adiabatic. The initial and boundary conditions of the beam can be expressed as[52,53]:

$$\begin{aligned} &T(z,t)=\beta(t)\\ &T(z,0)=0\\ &q(0,t)=0\\ &q(z,0)=0, \end{aligned} \tag{9}$$

in which $\beta(t)=\begin{cases}\frac{1}{2}+\frac{3}{4}\left(\frac{2t}{t^*-1}\right)-\frac{1}{4}\left(\frac{2t}{t^*}-1\right)^3 & \text{if } 0\le t\le t^*\\ 1 & \text{if } t\ge t^* \text{ for BCI}\\ 0 & \text{if } t\le t^* \text{ for BCII}\end{cases}$ is a third-order polynomial approximating a sudden change in the temperature.

3 | SOLUTION METHOD

Unlike other solution methods, DQM does the computation over the entire spatial–temporal domain (z-x plane) at one step. Therefore, to accommodate the whole boundary conditions accurately, the time step should be considered very small. Increasing the number of sampling grid points to capture the boundary conditions causes a few problems: (1) increasing the order of the system of equations; (2) increasing the running time to compute the state variables; (3) the considerable accumulation of numerical errors due to the weighting coefficient of sampling grid points.

To eliminate these drawbacks while keeping high-level accuracy, Shu[43] proposed an efficient temporal discretization approach based on block-marching in time and DQM discretization in both the spatial and temporal directions, as shown in Figure 2.[45] The same approach is used here to solve the nonlocal heat conduction in a nanostructure. More details of this procedure can be found in the literature.[43,47,48,54] The pth order derivative of the continuous function $f(z,t)$ in the spatial or temporal directions at an arbitrary sampling grid point z_i can be written as follows:

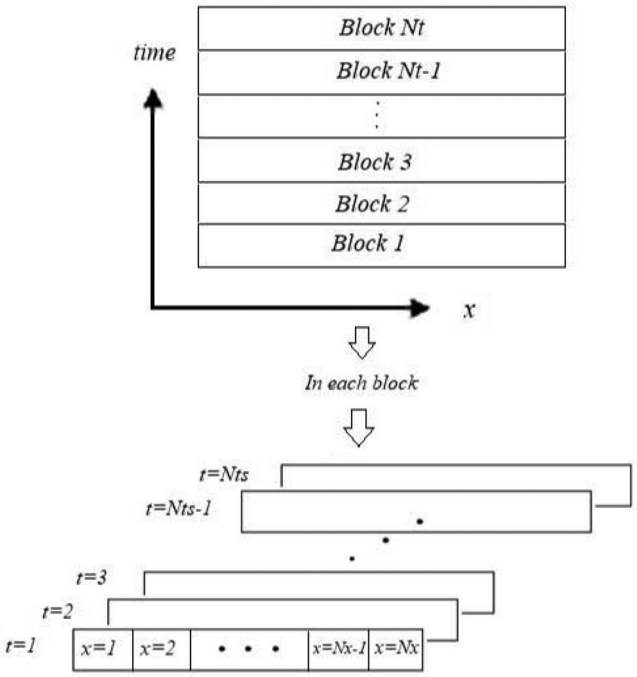

FIGURE 2 Configuration of block-marching technique and mesh point distribution in each block

$$\left.\frac{\partial f^p(z,t)}{\partial z^p}\right|_{z=z_i} = \sum_{k=1}^{N} C_{ik}^p f(z_{ik},t_j), \quad (i=1,2,...N_z, j=1,2,...N_t, p=1,2,...N_z-1) \tag{10}$$

$$\left.\frac{\partial f^p(z,t)}{\partial t^p}\right|_{t=t_i} = \sum_{k=1}^{N} D_{jk}^p f(z_{ik},t_j), \quad (i=1,2,...N_z, j=1,2,...N_t, p=1,2,...N_z-1), \tag{11}$$

where N_z and N_t are the number of sampling points along z and t directions, respectively. Also, C_{ik}^p and D_{jk}^p are the z_i and t_j dependent weight coefficients.

By considering the test functions as the Lagrange interpolation polynomials, the weighting coefficients of the first- and second-order derivatives are available in Ref [36], and they are defined, respectively, by

$$C_{ik}^1 = \frac{M^{(1)}(z_i)}{(z_i-z_k)M^{(1)}(z_k)}, \; for\, i\neq k, i,k=1,2,...,N \tag{12}$$

$$C_{ik}^2 = 2C_{ik}^1\left(C_{ii}^{(1)} - \frac{1}{z_i-z_k}\right), \; for\, k\neq i, i,j=1,2,...,N$$
$$C_{ii}^2 = -\sum_{k=1,i\neq k}^{N} C_{ik}^2, \tag{13}$$

where

$$M^{(1)}(z_i) = \prod_{m=1,m\neq j}^{(N)} (z_j - z_m). \tag{14}$$

3.1 | Nonlocal heat conduction

DQM is employed to discretize the temporal and spatial derivatives. The total temporal domain is divided into a set of time intervals and the obtained temperature at the end of each time interval is used as an initial condition for the next time interval. Thereby, in the beginning, the temperature and heat flux at a given control volume, P, at time, t, are obtained from the boundary conditions and then the value at time interval, $t+\Delta t$, is found, and will be considered as an initial condition for the next time step. All time intervals are thus connected, and the time history of temperature will be obtained. The DQM being applied to Equations (7, 8), the following equations at arbitrary sampling points z_i and t_j are then obtained:

$$k_{ij}\sum_{m=1}^{N_x} C_{im}^{z1} T_{mj} - l^2 \sum_{m=1}^{N_x} C_{im}^{z2} T_{mj} + \tau_q \sum_{n=1}^{N_t} D_{jn}^1 q_{in} + q_{ij} = 0 \tag{15}$$

$$\sum_{m=1}^{N_x} C_{im}^{z1} q_{mj} + \rho_{ij} C_{ij} \sum_{n=1}^{N_t} D_{jn}^1 T_{in} = g_{ij}. \tag{16}$$

The solutions of Equations (15 and 16) will be obtained by employing the Newton–Raphson method.

4 | RESULTS AND DISCUSSION

4.1 | Validation

To predict the temperature distribution, the DQM has shown good agreement in all nodes with the analytical solution,[55] as shown in Figure 3. The same values for the parameters are considered here as those in Ref [55]. The results are presented for the hyperbolic heat conduction in a slab which is heated on both sides with zero initial conditions at the nanoscale. The hyperbolic heat conduction in the Laplace domain is presented in Ref [53] and K_n is used to consider the effect of nonlocality.

4.2 | Numerical results and discussion

In the following calculations, the heat conduction-related parameters take these values, unless otherwise mentioned.

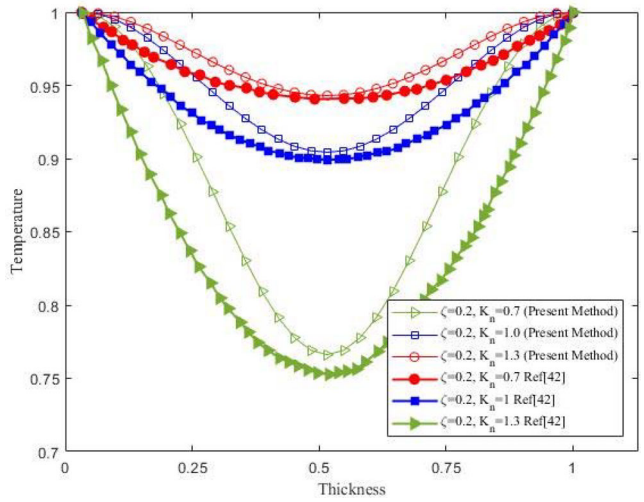

FIGURE 3 Comparison between two different solution methods, (1) differential quadrature method (present method) (2) Fourier transformation [Color figure can be viewed at wileyonlinelibrary.com]

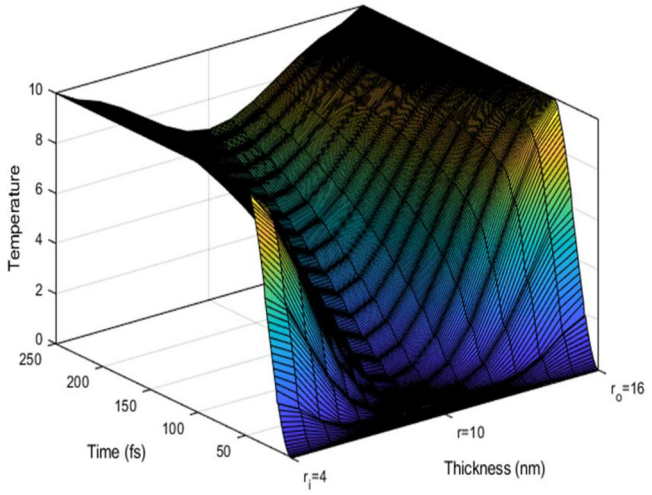

FIGURE 4 Time history of the temperature distribution at different points through the thickness [Color figure can be viewed at wileyonlinelibrary.com]

For nanobeam: $\rho = 1600$ kg/m^3, $t_o = 12*10^{-}7$ s, $C_p = 630$ J/K, $K = 30$, $r_i = 4*10^{-12}$ m, $r_0 = 16*10^{-12}$ m and $l = 2*10^{-8}$m. Here r_i and r_o are the inner and outer radii of the hollow cylinder, $r = (r_i + r_0)/2$.

Also, the number of sampling grid points for DQM is considered equal to 21, time increment (dt) is $1*10^{-15}$ s and $t^* = 5*10^{-15}$ s.

In Figures 4 and 5, we assumed that there is a thermal shock on both inner (r_i) and outer (r_o) surfaces of the cylinder. For the thermal shock, there is a 10°C increase in temperature in 50 fs and then it stays still. The fast rise in temperature at the boundaries (r_i and r_o) happens as a result of prescribed boundary conditions. The increase in the temperature in the middle parts of the thickness is slower than what? due to the time required for the heat flux to entirely reach and cover this area. Also, thermal waves can be seen in Figure 4, and they become weaker as time goes on.

Figure 6 indicates the effects of the thermal shock time duration (t^*) on the temperature distribution. As shown in Figure 6(A), $t^* = 0$ means that the temperature at the boundary is constant ($T = 10$), and it gives the highest value of the temperature throughout the thickness of the nanobeam (Figure 6(B)). By increasing the value of t^*, and plotting the temperature pattern at $t = 20$ fs, the lower temperature is obtained, as shown in Figure 6(B).

The temperature distributions through the thickness of the cylinder are presented in Figure 7 at different characteristic lengths. In Figure 7, the presence of the internal characteristic length prevents the temperature from exceeding the boundary temperatures, which is known as

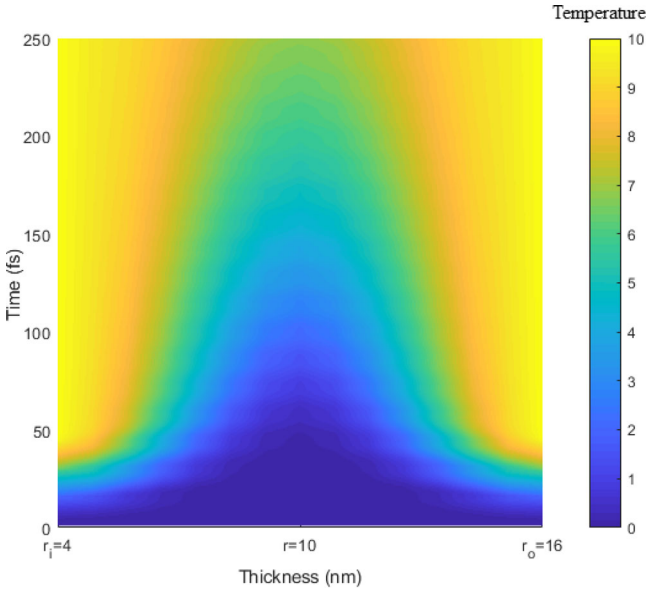

FIGURE 5 Heat transfer simulation in Matlab (Heatmap) [Color figure can be viewed at wileyonlinelibrary.com]

overshooting and may damage electrical devices if it is not handled correctly. Furthermore, the small value of the nonlocal length keeps the nonlocal effect within a physical domain contiguous to the imposed thermal shock at the boundary. As the characteristic length becomes conspicuous at a large value of the nonlocal length, the nonlocal effect escalates from the border and propagates within the medium.

Figure 8 depicts the temperature distribution at $t = 20$ fs for different relaxation times. The increase in thermal relaxation time causes a decrease in the thermal

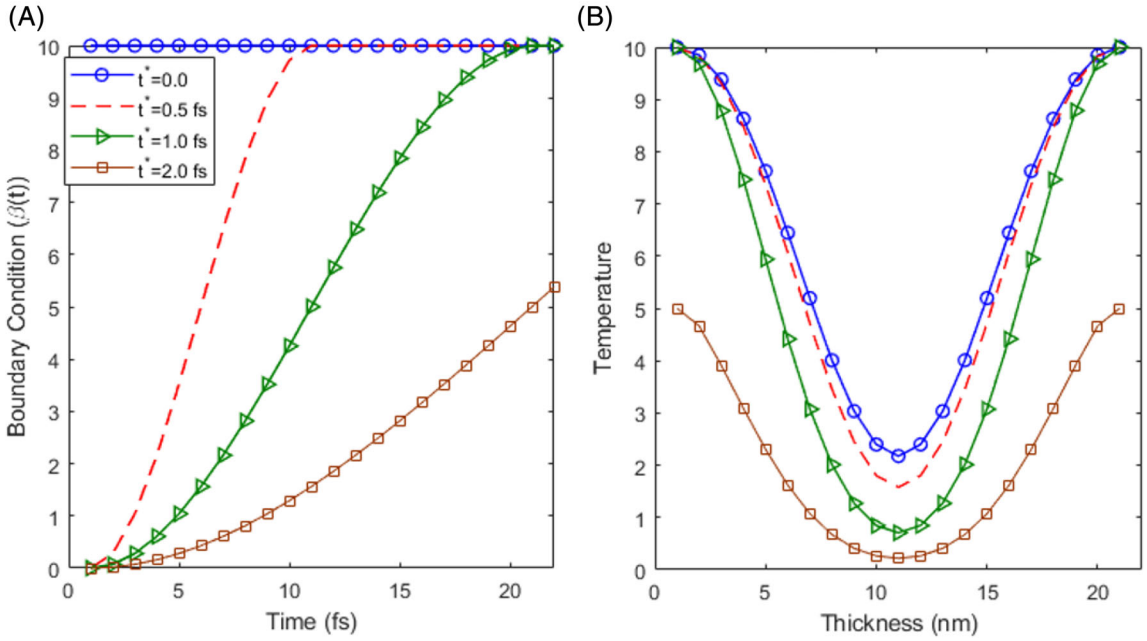

FIGURE 6 Temperature distribution through the thickness by changing the time duration of the thermal shock (t^*) (A) Boundary conditions, (B) temperature distribution across the thickness of the carbon nano-tube at $t = 20$ fs [Color figure can be viewed at wileyonlinelibrary.com]

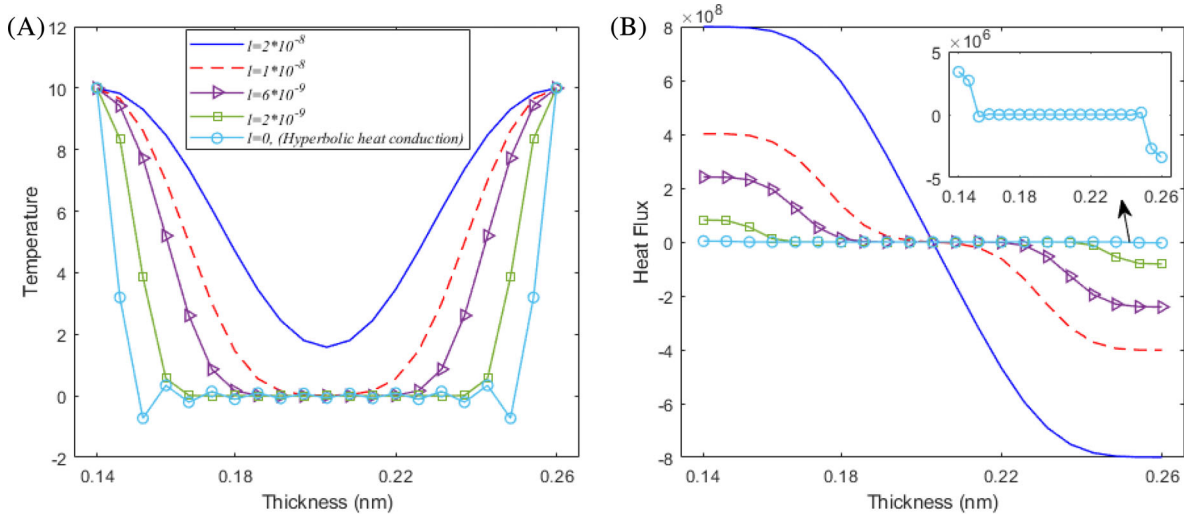

FIGURE 7 Effects of the characteristic length (l) on the temperature distribution at $t = 20$ fs [Color figure can be viewed at wileyonlinelibrary.com]

wave propagation speed and thereby decreases the change in temperature away from the imposed boundary. As shown in Figure 8, for the highest value of the relaxation time, $\tau_0 = 12 * 10^{-4}$ s, a large proportion of the thickness has not experienced the thermal shock and the temperature has remained zero. On the contrary, for $\tau_0 = 12 * 10^{-7}$ s, which is the smallest value of relaxation time, the whole thickness domain has been affected by the thermal shock at the boundary.

The temperature distribution through the thickness for the second type of boundary condition is presented in Figure 9. Figure 9 shows that the temperature in the area close to the inner (r_i) and outer (r_o) surfaces first increase very fast in the heating stage ($0 < t < 10$ fs). Then the heat source at the boundary disappears, and the temperature becomes zero in these areas. Although we have removed the heat source from the boundary, the effects of thermal shock are still observed in the middle parts of the

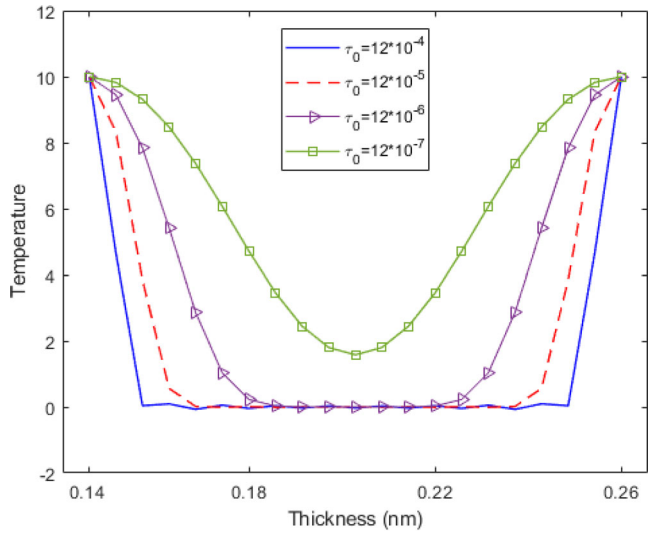

FIGURE 8 Effects of the relaxation time on the temperature distribution at $t = 20$ fs [Color figure can be viewed at wileyonlinelibrary.com]

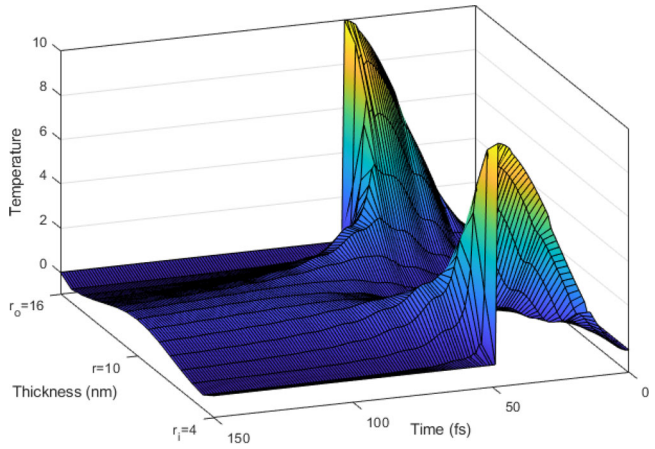

FIGURE 9 Temperature history of the temperature, BC: II [Color figure can be viewed at wileyonlinelibrary.com]

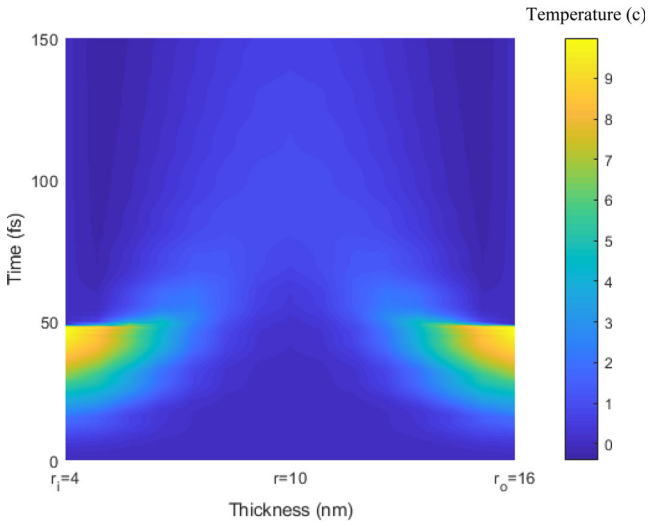

FIGURE 10 Visualizing temperature with single heatmap, BC: II [Color figure can be viewed at wileyonlinelibrary.com]

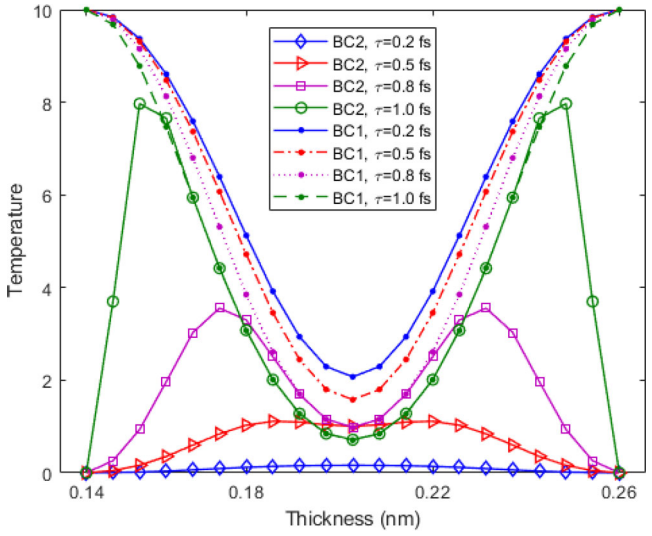

FIGURE 11 Transition from non-Fourier heat conduction to Fourier heat conduction at $t = 20$ fs [Color figure can be viewed at wileyonlinelibrary.com]

thickness. The heat transfer within the media can be seen in Figure 10. It is illustrated that although the temperature at the boundary is set to zero after 50 fs, the heat transfer continues and tends to move toward the center of the media.

Figure 11 is a comparison between the effects of two different boundary conditions on the temperature distribution within the nano-cylinder. In the case of $\tau_0 = 0.8$ fs and 1 fs, there has been some exciting results. We observed that for two different boundary conditions, the temperature of some regions in the middle of the thickness is identical. We can justify this instance by considering the fact that temperature in the area away from the imposed boundary, at the initial stages, depends more on the characteristic length and relaxation time. The boundary conditions determine the limits of the temperature, and the characteristic length along with the relaxation time define how fast the medium can reach these limits.

Figure 12 plots the variation of temperature distribution at $t = 20$ fs through the thickness of the beam for different thickness ratios (r_o/r_i). It shows that the temperature gradually decreases with increasing thickness ratio. For the shortest value of the thickness ratio, the whole thickness has experienced a change in temperature, but for the larger value of the thickness ratio, the temperature at the area around the center ($r = r_i + r_o/2$) remains indentical.

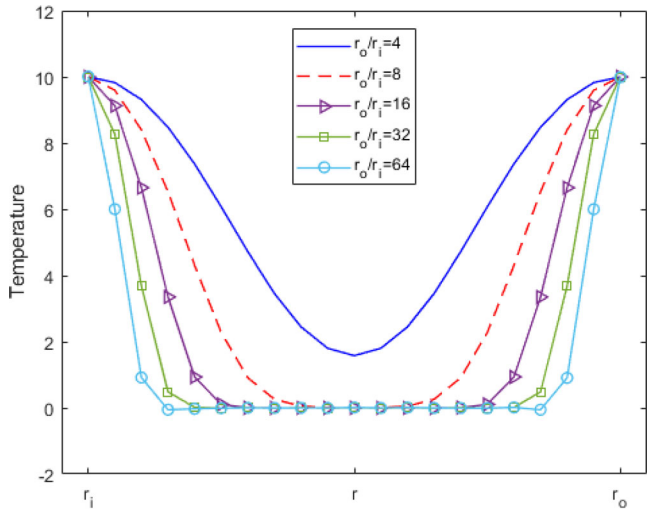

FIGURE 12 Effects of the thickness ratio on the temperature distribution [Color figure can be viewed at wileyonlinelibrary.com]

5 | CONCLUSION

A semi-analytical solution for the modified Guyer-Krumhansl equation is addressed for a nanobeam modeled as a cylindrical shell using the DQM. The differential quadrature approach is employed to develop a new solution method leading to a more straightforward solution. The method enables to assess the role of boundary conditions and material properties in two and three-dimensional problems. The linear effect of nonlocality was extended in space under the direct impact of thermal lagging in time. For the large values of relaxation time, the time delay effect is restricted to a physical domain close to the boundary. Decreasing the value of the time delay pushes the thermal waves forward. Furthermore, when the characteristic length is small, there is a sharp decline in temperature near the boundary, while the temperature in the center of the cylinder is identical to that obtained from the hyperbolic heat conduction. A similar phenomenon happens for the heat flux. The small characteristic length confines the effects of the interactions between boundary and energy carriers within a physical domain near the boundary.

ACKNOWLEDGMENT

The authors thank the Natural Sciences and Engineering Research Council (NSERC) of Canada for the financial support to the present work.

ORCID

Amin Pourasghar https://orcid.org/0000-0003-4941-0943

REFERENCES

[1] S. Li, Y. Feng, Y. Li, W. Feng, K. Yoshino, *Carbon* **2016**, *109*, 131.
[2] J. Li, N. Kurra, M. Seredych, X. Meng, H. Wang, Y. Gogotsi, *Nano Energy* **2019**, *56*, 151.
[3] P. Yu, S. Q. Xiao, X. Lu, C. Zhou, L. Yang, Z. W. Liu, B. W. Liu, W. Xu, C. C. Jia, Q. XuanHui, *J. Alloys Compd.* **2019**, *782*, 1015.
[4] K. Krishnamoorthy, V. K. Mariappan, P. Pazhamalai, S. Sahoo, S.-J. Kim, *Nano Energy* **2019**, *59*, 453.
[5] Y. S. Song, J. R. Youn, *Carbon* **2005**, *43*, 1378.
[6] Z. Špitalský, L. Matějka, M. Šlouf, E. N. Konyushenko, J. Kovářová, J. Zemek, J. Kotek, *Polymer Compos.* **2009**, *30*, 1378.
[7] S. Mondal, N. Sarkar, N. Sarkar, *J. Thermal Stress.* **2019**, *42*, 1035.
[8] A. Pourasghar, M. Homauni, S. Kamarian, *Polym. Compos.* **2016**, *37*, 3175.
[9] M. Gupta, S. Mukhopadhyay, *J. Thermal Stress.* **2019**, *42*, 1123.
[10] A. I. Aria, M. I. Friswell, *Compos. Part B* **2019**, *166*, 233.
[11] A. M. Fattahi, B. Safaei, E. Moaddab, *Steel Compos. Struct.* **2019**, *32*, 281.
[12] N. S. Al-Huniti, M. A. Al-Nimr, *J. Thermal Stress.* **2019**, *27*, 607.
[13] S. Kamarian, M. Bodaghi, R. B. Isfahani, M. Shakeri, M. H. Yas, *Mech. Based Design Struct. Mach. Int. J.* **2020**, *49*, 217.
[14] S. Kamarian, M. Bodaghi, R. B. Isfahani, J. Song, *J. Sandwich Struct. Mater.* **2020**. https://doi.org/10.1177/1099636220935557.
[15] F. Fana, S. Sahmani, B. Safaei, *Compos. Struct.* **2021**, *255*, 112969.
[16] R. Moradi-Dastjerdi, K. Behdinan, *Aerospace Sci. Technol.* **2020**, *106*, 106142.
[17] K. Behdinan, R. Moradi-Dastjerdi, B. Safaei, Z. Qin, F. Chu, D. Hui, *Nanotechnol. Rev.* **2020**, *9*, 41.
[18] V. V. Deshpande, S. Hsieh, A. W. Bushmaker, M. Bockrath, S. B. Cronin, *Phys. Rev. Lett.* **2009**, *102*, 105501.
[19] C. Liang, Z. Huang, S. Kumar, *Appl. Phys. Lett.* **2013**, *103*, 123110.
[20] M. Hartmann, G. Mahler, O. Hess, *Phys. Rev. Lett.* **2004**, *93*, 080402.
[21] S. Biswas, *J. Thermal Stress.* **2020**, *43*, 284. https://doi.org/10.1080/01495739.2019.1699482.
[22] V. A. Ermakov, A. V. Alaferdov, A. R. Vaz, A. V. Baranov, S. A. Moshkalev, *Nanotechnology* **2013**, *24*, 155301.
[23] P. E. Hopkins, M. Baraket, E. V. Barnat, T. E. Beechem, S. P. Kearney, J. C. Duda, J. T. Robinson, S. G. Walton, *Nano Lett.* **2012**, *12*, 590.
[24] Y. K. Koh, M.-H. Bae, D. G. Cahill, E. Pop, *Nano Lett.* **2010**, *10*, 4363.
[25] C. Zhang, W. Chen, Y. Tao, W. Zhao, S. Cai, C. Liu, Z. Ni, D. Xu, Z. Wei, J. Yang, K. Bi, Y. Chen, *Carbon* **2017**, *115*, 665.
[26] B. Mortazavi, T. Rabczuk, *Carbon* **2015**, *85*, 1.
[27] K.-Q. Peng, X. Wang, L. Li, Y. Hu, S.-T. Lee, *Nano Today* **2013**, *8*, 75.
[28] C. Cattaneo, *Comptes Rendus* **1958**, *247*, 431.
[29] P. Vernotte, *Compte Rendus* **1961**, *252*, 2190.
[30] A. Pourasghar, Z. Chen, *Waves Random Complex Media*, 1. **2020**, https://doi.org/10.1080/17455030.2020.1813351.
[31] A. Pourasghar, Z. Chen, *Heat Mass Transfer* **2020**, *56*, 1171.
[32] S. L. Sobolev, *Int. J. Heat Mass Transfer* **1994**, *37*, 2175.

[33] D. Y. Tzou, *Int. J. Heat Mass Transfer* **1995**, *38*, 3231.
[34] R. A. Guyer, J. A. Krumhansl, *Phys. Rev.* **1966**, *148*, 766.
[35] R. A. Guyer, J. A. Krumhansl, *Phys. Rev.* **1966**, *148*, 778.
[36] L. Wang, J. Xu, J. Wang, *Int. J. Heat Mass Transfer* **2018**, *118*, 1284.
[37] X. Mingtian, *Int. J. Thermal Sci.* **2018**, *134*, 594.
[38] C. Shu, L. Wang, Y. T. Chew, *Int. J. Numer. Methods Fluids* **2003**, *43*, 345.
[39] Z. Zong, K. Y. Lam, *Comput. Mech.* **2002**, *29*, 382.
[40] T. C. Fung, *Computer Methods Appl. Mech. Eng.* **2002**, *191*, 1311.
[41] C.-N. Chen, *Computers Math. Appl.* **2004**, *47*, 91.
[42] M. Tanaka, W. Chen, *Appl. Math. Model.* **2001**, *25*, 257.
[43] C. Shu, Q. Yao, K. S. Yeo, *Computer Methods Appl. Mech. Eng.* **2002**, *191*, 4587.
[44] A. Pourasghar, Z. Chen, *Phys. B Condens. Matter* **2019**, *564*, 147.
[45] A. Pourasghar, Z. Chen, *Int. J. Eng. Sci.* **2019**, *137*, 57.
[46] A. Pourasghar, Z. Chen, *Int. J. Solids Struct.* **2019**, *163*, 117.
[47] A. Pourasghar, R. Moradi-Dastjerdi, M. H. Yas, A. Ghorbanpour Arani, S. Kamarian, *Polymer Compos.* **2018**, *39*, 1161.
[48] A. Pourasghar, Z. Chen, *Compos. Part B* **2016**, *99*, 436.
[49] D. Y. Tzou, *Int. J. Heat Mass Transfer* **2011**, *54*, 475.
[50] R. Barretta, M. Čanađija, F. M. de Sciarra, *Compos. Struct.* **2019**, *225*, 104.
[51] Y. Jun Yu, Z.-N. Xue, C.-L. Li, X.-G. Tian, *Compos. Struct.* **2016**, *146*, 108.
[52] A. D. Polyanin, V. F. Zaitsev, *Handbook of Nonlinear Partial Differential Equations*, Chapman and Hall/CRC, United Kingdom **2016**.
[53] C. A. Dorao, *J. Comput. Appl. Math.* **2009**, *231*, 637.
[54] A. Pourasghar, S. Kamarian, *J. Vib. Control* **2015**, *21*, 2499.
[55] Y. Jun, C.-L. L. Yu, Z.-N. Xue, X.-G. Tian, *Phys. Lett. A* **2016**, *380*, 255.

How to cite this article: Pourasghar A, Yang W, Pasini D, Chen Z. Nonlocal heat conduction in single-walled carbon nanotubes. *Polymer Composites*. 2021;1–9. https://doi.org/10.1002/pc.26068